

Mixing ventilation coupled with personalized sinusoidal ventilation: Optimal frequency and flow rate for acceptable air quality



Douaa Al Assaad^a, Kamel Ghali^a, Nesreen Ghaddar^{a,*}, Carine Habchi^b

^a Mechanical Engineering Department, American University of Beirut, P.O. Box 11-0236, Beirut 1107-2020, Lebanon

^b Mechanical Engineering Department, Faculty of Engineering, Lebanese University, Branch 2 Roumieh, Lebanon

ARTICLE INFO

Article history:

Received 14 June 2017

Received in revised form 30 August 2017

Accepted 31 August 2017

Available online 6 September 2017

Keywords:

Personalized ventilation
Mixing ventilation
Computational fluid dynamics
Thermal comfort
Indoor air quality
Energy savings

ABSTRACT

This study investigates and optimizes the performance of a localized dynamic personalized ventilation (PV) coupled with a mixing ventilation system (MV). A transient computational fluid dynamics model (CFD) was used to assess the velocity, temperature and CO₂ fields around the occupant microclimate. The CFD model was also coupled with a transient bio-heat model to compute the segmental skin temperatures, overall thermal sensation and comfort. The model was then validated experimentally by using a thermal manikin in a climatic chamber representing an occupant in a typical office space. There was a good agreement between experimental and predicted values. The model was then used to optimize the operating frequency and average flowrate for the best thermal comfort and ventilation effectiveness. The optimal operating conditions of the localized dynamic airflow for a background temperature of 26 °C and a PV temperature of 22 °C, were for an average supply flowrate of 7.5 L/s and a frequency of 0.94 Hz providing an overall comfort of 0.95 (comfortable) on a comfort scale from very uncomfortable at –4 to very comfortable at +4 and a ventilation effectiveness of 77%. These conditions were able to provide the best compromise between comfort and air quality. They were also able to reduce energy costs by 21.34% compared to a constant personalized ventilation system providing the same levels of comfort.

© 2017 Elsevier B.V. All rights reserved.

1. Introduction

The purpose of heating, ventilation, and air conditioning (HVAC) systems is to provide occupants in built-in environment with a good level of thermal comfort for their well-being and productivity and a good indoor air quality (IAQ) to reduce human health risks. Thermal comfort is generally met by bringing air room temperature to adequate level through mixing of the supplied air with the room air and also by displacement of the warm and polluted air and replacing it with cool and clean air. On the other hand, good IAQ is achieved by supplying sufficient amount of fresh air to dilute contaminants in the space. To meet both comfort and IAQ, a large percentage of cool fresh air should be brought into the space which entails high energy consumption. In other words, requirements are met in conventional air conditioning systems by maintaining the space at a constant temperature and a homogenous air quality by a mixed fresh-return air distribution system. In such design, the individual environmental preference is not accommodated since room temperature is controlled by single thermostat. This may lead in

an open space to the failure in satisfying the thermal comfort and indoor air quality needs of all occupants [1,2].

Efforts have been made in the HVAC industry in order to decrease cooling requirements in spaces while still assuring good air quality needs are made. Recent approaches focused on localized air conditioning where conditioned air flows around the occupant using different types of personalized ventilation (PV) with the air conditioning system. For efficient air conditioning and effective delivery of fresh air, the usage of personalized ventilation (PV) was proposed by Halvonova et al. [3] and by Li et al. [4] at adjustable flow rates and temperatures to meet the occupants comfort and air quality needs. Sekhar et al. [5] performed an energy analysis on desk mounted PV in hot and humid climates in conjunction with a background air conditioning system and reported 15–30% of energy savings. Yang et al. [6] used ceiling mounted PV with the Air Terminal Device (ATD) placed above the head of the occupant, and reported energy savings of 15.44% for an indoor air temperature of 26 °C and 23.5 °C for PV. Another approach was studied by Makhoul et al. [7] who integrated a PV ceiling nozzle with a task ventilation nozzle and reported substantial energy savings of 30%, Makhoul et al. [8] also improved the previous system by adding desk fans to the office space, further energy savings of 13% and a ventilation efficiency of 32% were reported. Schiavon et al. [9] reported about 51%

* Corresponding author.

E-mail address: farah@aub.edu.lb (N. Ghaddar).

energy savings when PV was coupled with mixing ventilation compared to a standalone mixing system providing the same indoor air quality (IAQ). Therefore, localized cool fresh air cools the microclimate in the vicinity of each occupant while reducing energy costs. Nevertheless, for a PV to be effective in providing good ventilation and breathable air, the PV jet should be able to reach the breathing zone of the occupant with minimal mixing and entrainment of contaminated room air.

Most studies on PV [3–9] were concerned with assessing the effect of delivery of a constant flowrate of cool fresh air from the task ventilation on energy savings. Recently, few studies investigated the effect of varying airflow amplitude and frequency on occupant thermal comfort and energy saving [10–13]. In fact, intermittent airflow can also enhance comfort by mimicking natural outdoor conditions. Ghali et al. [10] performed outdoor experiments on human subjects and reported that the average thermal comfort improved with the change in wind frequency. Furthermore, providing airflow intermittently can help decrease PV energy costs even further by reducing the amount of fresh air to be cooled by the system and lowering the fans' power consumption as reported by Kabanshi et al. [11] who used ceiling mounted Air Jet Diffusers (AJD) supplying dynamic airflow in an ON-OFF pattern. Uğursal et al. [12] and Tanabe et al. [13] conducted indoor human subject experiments to investigate the performance of localized dynamic airflow at two different periods of 30 s and 60 s. Both studies reported that a period of 30 s provided more perceived thermal comfort. Zhou et al. [14] performed measurements in offices under natural and mechanical ventilation where occupants were subjected to fluctuating airflow in cool conditions. They concluded that room airflow felt most uncomfortable when the frequency ranged between 0.2 Hz and 0.6 Hz. However, none of these studies considered the effect of different supply flow rates and frequencies on thermal comfort or the effect of the varying airflow pattern on the IAQ. Accelerating and decelerating airflow could create turbulence and enhance the mixing of the contaminants in the breathing zone. This would decrease the ventilation efficiency of the PV and therefore deteriorate the air quality in the microclimate of the occupant. On one side, intermittent PV succeeds in bringing comfort [15] but on the other hand, it may compromise IAQ. To the authors' knowledge, no previous research has addressed the use of intermittent PV to aid mixed ventilation and its impact on air quality.

This study investigates the performance of localized dynamic airflow with the purpose of optimizing the supply frequency and minimum and maximum velocity for good thermal comfort and good IAQ at reduced energy cost. A PV supplying a horizontal sinusoidal airflow is proposed to assist a mixing ventilation (MV) system. A 3-D computational fluid dynamics (CFD) model of MV-conditioned space with PV nozzle is developed. The CFD model is validated with experiments performed on a thermal manikin by comparing segmental skin temperatures and the concentration of CO₂ in the breathing zone at specified conditions of temperature, flow rates and frequency. A parametric study is then conducted to evaluate the system's ability in assuring a good compromise between good IAQ, thermal comfort and energy savings compared to a standalone mixing ventilation.

2. Methodology

2.1. System description

The schematic diagram of the MV+PV system is shown in Fig. 1(a). The considered room is a typical office space equipped with a conventional MV system served by its own air handling unit AHU. It has two inlet diffusers supplying mixed air into the room and an exhaust diffuser handling the return air to adjust the

macroclimate temperature. The MV system is assisted by a personalized ventilation composed of a horizontal nozzle with a fan installed inside the duct. The PV system withdraws cooled clean fresh air from an adjoining fresh air source and supplies it intermittently conditioning the microclimate around the occupant. A more detailed schematic of the PV system can be seen in Fig. 1(b): The PV is placed at a typical horizontal distance δ ($=40$ cm) [16] from the occupant which is represented by a multi segmented manikin while the air supply varies between a minimum and a maximum flowrate at a variable frequency f .

2.2. CFD model

In this study, the MV is coupled with a localized dynamic airflow directed towards the face of the occupant thus creating transient periodic conditions. This problem is complex since it incorporates different physical mechanisms that affect velocity, temperature and concentration fields in the vicinity of the thermal manikin. In addition, the flow field is affected by the rising thermal plumes from the thermal manikin, the wall plumes, the supply and exhaust mixed ventilation airflow, the recirculating room air, and the intermittent PV jet flow. It is noteworthy that the flow field can be even more complicated with the inclusion of breathing from the thermal manikin, however it was found to be negligible. For instance, Melikov et al. [17] reported that at 2–3 cm away from the thermal manikin, the velocities of inhalation and exhalation are very small and do not interfere with the thermal plume rising from the occupant with the PV jet penetrating the plume at a speed much higher than that of the respiratory process.

Consequently, this study does not include a breathing thermal manikin. Nevertheless, the flow field is still very complex and calls for the use of a 3-D CFD simulation tool to resolve for the distribution of different dependent variables. Previous studies [8,9] employed 3-D CFD modeling to accurately predict velocity, temperature and contaminants distribution in the space and obtained good results, which is why this approach is used to assess the effectiveness of localized dynamic airflow in conjunction with the mixing ventilation system under different operating conditions. The results of the CFD model are validated through experiments. Following the CFD model validation, it is used to simulate a parametric study in a regular office space where the above-mentioned parameters are varied in order to study the effectiveness of the MV + PV system in delivering good indoor air quality and thermal comfort at minimum energy costs.

2.2.1. Airflow modeling

The commercial software ANSYS Fluent [18] is selected to visualize the flow field of the indoor environment as shown in Fig. 2. Proper prediction of the properties of the flow such as the turbulence models, buoyancy effects and boundary layers near the surfaces, the airflow temperature, velocity and CO₂ concentration fields is important to understand the flow physics. The mesh should be able to capture the shear layer entrainment and the thermal plumes at some surfaces as well as the fluid and thermal boundary layers coming from the manikin: Inflation layers are used to predict the flow behavior at the boundary layers, inflation layers should be selected such that the dimensionless number y^+ ranges between 0.8 and 4 to solve for the viscous sub-layer [19].

The RNG k - ϵ model with enhanced wall treatment is used to model turbulence; it is characterized by its accuracy and good predictability of jet spreading rate and the behavior of recirculated air.

To account for buoyancy effects, the Boussinesq approximation is selected and the species transport equation is used to calculate the CO₂ concentration field. The momentum, energy, k , ϵ , turbulence and species transport equations are discretized using second

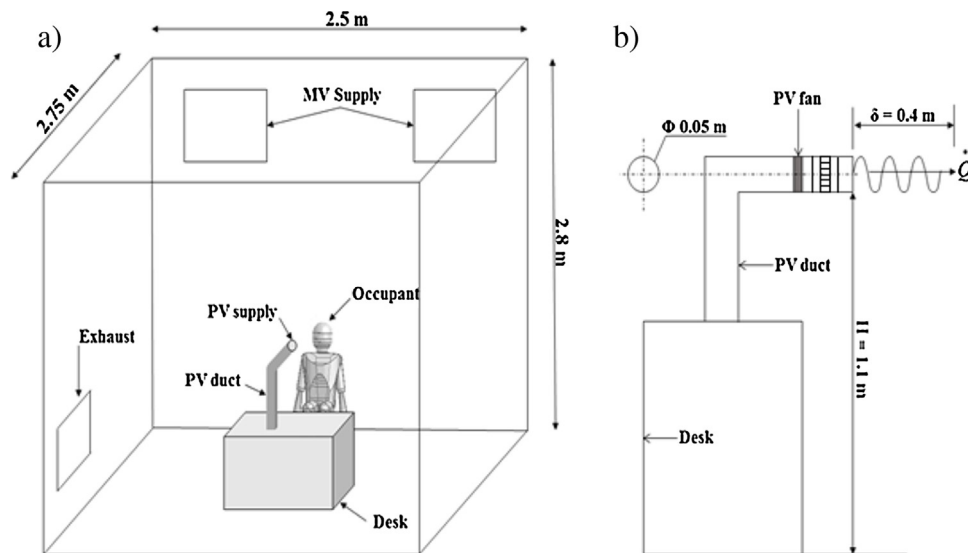


Fig. 1. Schematic diagram of (a) PV+ mixing system and (b) detailed schematic of PV.

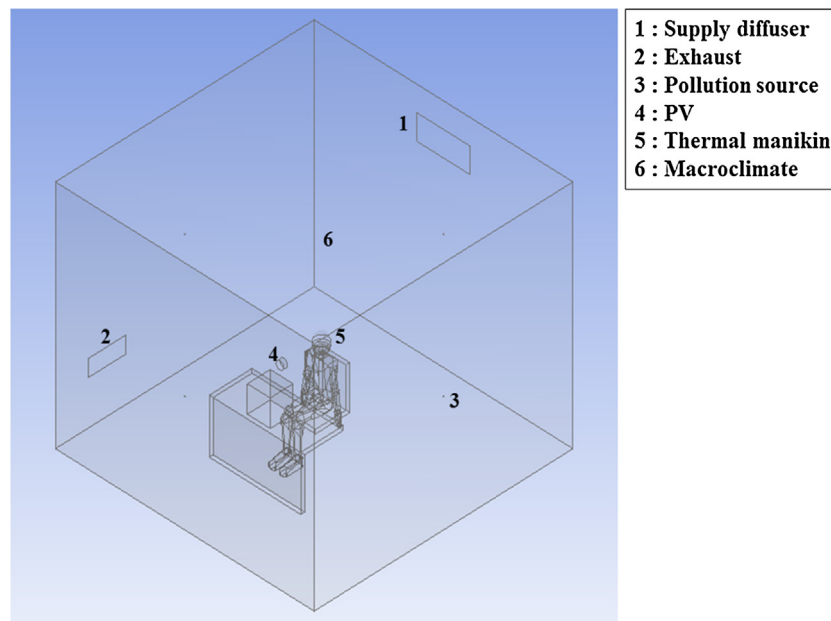


Fig. 2. The computational domain used in ANSYS: (1) supply diffusers (2) exhaust (3) pollution source (4) personalized ventilation (5) thermal manikin (6) macroclimate.

order upwind scheme. Since unsteady conditions are present, the solver is set to transient and second order implicit time stepping is used with a time step of 0.01 s. The “PRESTO!” scheme is used to discretize the pressure and the latter is coupled with velocity using the PISO algorithm. Numerical convergence is reached when scaled residuals are less than 10^{-5} and the net heat flux less than 1% of the total heat gained in the domain [19].

The boundary faces are set to different element sizes using tetrahedral unstructured grid, a face size of 1.5 cm was assigned for the manikin, and 2 cm for the walls. This assures an independent grid with relative error less than 5% to ensure that the solution is independent of the mesh chosen. The final mesh of the space with dimensions of 2.8 m \times 2.75 m \times 2.5 m is shown in Fig. 3. It is characterized by 303,533 nodes and 1,056,484 elements. The different mesh cases with relative errors can be seen in Table 1.

2.2.2. Boundary conditions

In order to obtain accurate results in the CFD simulations concerning airflow properties, thermal and velocity fields, proper

Table 1
Grid independence testing using 5 different mesh cases.

	Face sizing (cm) Manikin/walls	Number of elements	Maximum relative difference in the predicted values of temperature and velocity values with previous mesh values (%)
Mesh 1	2/8	152395	–
Mesh 2	2/5	228592	44.62%
Mesh 3	1.5/3	480478	12.1%
Mesh 4	1.5/2.5	660302	5.3%
Mesh 5	1.5/2	1056484	4.2%

selection of boundary conditions is crucial. The supply diffuser is set to a constant velocity inlet, as for the PV supply inlet, a user defined function UDF is introduced in order to model the sinusoidal airflow presented in equation (2) where $V(t)$ is the variable velocity function, \bar{V} is the mean velocity characterized by a peak velocity V_1 and a

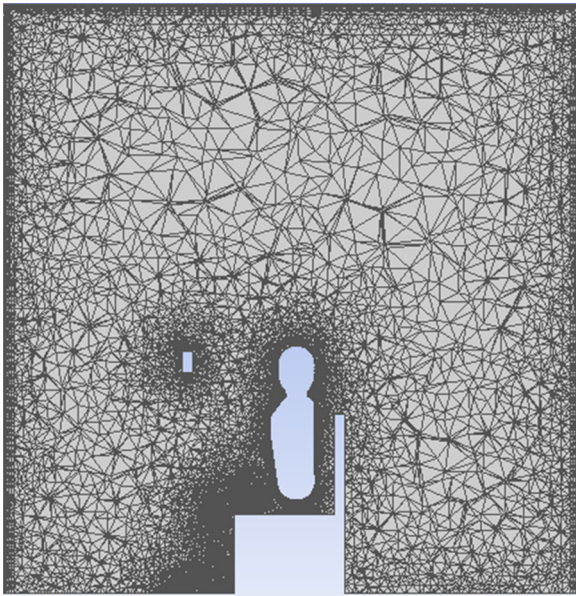


Fig. 3. Mesh generation of the computational domain.

minimum velocity V_2 , f is the airflow frequency and t denotes time [14].

$$V(t) = \bar{V} + \left(\frac{V_2 - V_1}{2} * \sin(2.\pi.f.t) \right) \quad (2)$$

The velocity magnitude and direction, airflow temperature, turbulence intensity and hydraulic diameter are set as input boundary conditions at the mixing diffusers and PV nozzle. The exhaust diffuser is set as outlet and zero gauge pressure. Finally, the walls and the ceiling are set to constant heat flux. To create a uniform generation of CO_2 inside the space, CO_2 sources were placed in the center of each wall.

2.2.3. Bio-heat coupling

The occupant in the room is subjected to two airflows; the first originates from the MV system. The second one is due to the PV sinusoidal jet which is restricted to the occupant upper body segments, which creates asymmetrical air conditions around these segments, therefore it is expected to have different cooling effects and variations in skin temperature for upper body parts, while the other segments remain in uniform conditions.

In order to assess these effects on thermal comfort, a transient bio heat model which can capture the time variations of skin temperatures is needed. The transient bio-head model of Othmani et al. [20] is used and is coupled with the CFD model in ANSYS to predict the thermal response of the occupant based on modeled physiology. The bio-heat model divides the body into 11 segments (head, chest, back, abdomen, back, buttocks, upper arm, lower arm, thighs, calves, and feet), it takes as input the environmental conditions including ambient air temperature and the convective heat transfer coefficients near each body segments and outputs the segmental skin temperatures. The transient bio-heat model of Othmani et al. [20] predicts accurately the segmental skin temperatures and core temperatures as a function of metabolic rate, environmental conditions and time.

The coupling between transient CFD and bio-heat models is shown in Fig. 4 where the manikin in the CFD model was initiated with conventional skin temperatures. The ambient air temperatures and convective heat transfer coefficients were used as input for the transient bio-heat model. It is noted that near the upper body segments (head, chest, abdomen, upper arms) where transient conditions are present, the temperature and heat transfer

coefficients are time dependent. The bio-heat model outputs appropriate skin temperatures. This perturbed stabilized residuals, thus the CFD model is simulated until residuals are stabilized again. This coupling procedure was repeated until the relative error between two consecutive iterations is smaller than 10^{-3} . The bio-heat model correlates the segmental skin temperature and core temperature as well as their rate of change to local segmental comfort and overall comfort and sensation based on Zhang et al. empirical model based on human subject experiments [21–23]. In transient environmental conditions, the bio-heat model will predict the rate of change of skin temperature which is directly related to the transient comfort model of Zhang et al. [21–23].

The thermal comfort scale of Zhang et al. [21–23] varied between -4 (very uncomfortable) to $+4$ (very comfortable) with 0 indicating just comfortable, while the thermal sensation scale varied from -4 (very cold) to $+4$ (very hot). When convergence in the coupling is reached, the obtained segmental skin temperatures were integrated with the model of Zhang et al. [21–23] to predict the local and overall thermal sensation and comfort.

2.2.4. Air quality modeling

To evaluate ventilation efficiency and measure the degree of mixing between the periodic PV fresh air and the surrounding contaminated room air, CO_2 is used as tracer gas [19]. Melikov et al. [24] introduced several indices to evaluate the ability of the PV jet in providing air quality needs. The index, which is adopted in this work, is the air quality index AQI denoted by ε_V and evaluates ventilation efficiency of the personalized ventilation. This index is calculated at the breathing zone of the occupant. The breathing zone (BZ) is defined as a control volume taking the shape of a sphere having a radius of 1 cm located at 2.5 cm away from the manikin's nose. The index ε_V was calculated using the following equation:

$$\varepsilon_V = \frac{C_R - C_{BZ}}{C_R - C_{Fr}} \quad (2)$$

Where C_R ; is the concentration of contaminant in the exhaust room air, C_{BZ} is the concentration in the breathing zone and C_{Fr} is the mean concentration in the fresh air supply. The higher this index is, the better the ventilation efficiency and the IAQ.

2.2.5. Choice of frequency, average flowrate and supply temperature

A dynamic airflow is characterized by its perceptible range of fluctuation frequency, the range of associated amplitudes and mean velocities determined by a given minimum and maximum jet flow. Therefore, it is important to determine the dynamic jet air flow characteristics and their ranges for both the experimental work and the simulations where the jet should be able to reach the breathing zone and penetrate the occupant thermal plume. In addition, acceptable ranges should be established of temperature of the surrounding air and the cooling jet within which thermal comfort is maintained.

There has been a number of studies on human thermal comfort at several frequencies of dynamic airflow in both outdoor and indoor spaces. The outdoor wind frequencies of 0.15, 0.25 and 0.35 Hz were reported in the study of Ghali et al. [10] as the prevailing outdoor frequencies during an average hot summer day. Their results showed that the overall comfort improved with the increase of wind frequency. In indoor environments, the study of the effect of flow frequency on comfort was carried out in neutral to cool and in warm thermal environments. According to Zhu et al. [25], the fluctuating airflow is defined by the range of perceptible frequency felt by the occupant, which lies between a lower limit of 0.1 Hz and an upper limit of 1 Hz. Several experiments were conducted in different ambient conditions to find the comfort range between these two limits. Fanger et al. [26] reported that under cool indoor

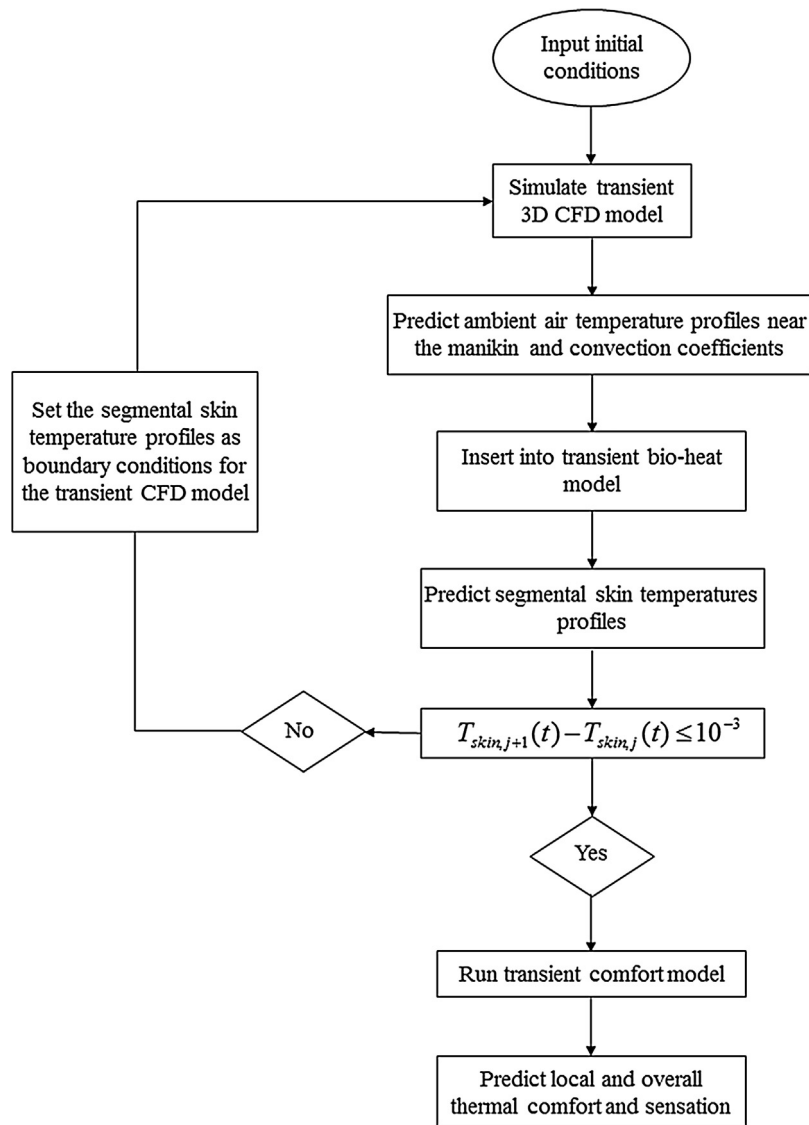


Fig. 4. Flow chart for the coupling of the CFD model with the transient bio-heat and comfort model.

conditions, discomfort reached a maximum at frequencies ranging between 0.3 Hz and 0.5 Hz. Zhou and Melikov [14] reported a range of frequencies between 0.2 Hz and 0.6 Hz; broader than the range found by Fanger et al. [26]. However, both studies show that under cool to neutral conditions, higher frequencies can cause discomfort and feelings of draft. On the contrary, in warm indoor conditions, such an airflow may induce feelings of comfort. As a matter of fact, Huang et al. [27] studied thermal comfort in warm indoor conditions (28 and 30 °C) and reported that a higher range of 0.5–1 Hz provided cooling and comfort.

Based on previous studies, it is well established that a fluctuating airflow trigger comfort conditions depending on the airflow temperature and the room background temperature. In this study, the conditions in the space are from neutral to warm while the PV jet temperature is cool. For these conditions, three frequencies of 0.3 Hz, 0.5 Hz and 1 Hz, were selected based on the values found by Fanger et al. [26] (0.3–0.5 Hz) and Huang et al. [27] (0.5–1 Hz) in order to evaluate thermal comfort.

A dynamic airflow is characterized by the jet velocity, which is defined by an average, a minimum and a maximum. The average flowrate was varied according to typical average flowrates used in PV airflow applications which range between 3 and 10 L/s [24].

For this study, 3 average flowrates were taken into consideration: 3.5 L/s, 5 L/s and 7.5 L/s. As for the choice of minimum velocity, it should be selected such that the supply jet can still penetrate the thermal plume of the occupant to deliver cool fresh air and provide comfort.

2.3. Experimental setup

Experiments were conducted on a thermal manikin in a conditioned climatic chamber using MV + PV to validate the CFD model results on predicted values of segmental skin temperature of the manikin and ventilation efficiency in the breathing zone.

The experimental setup consists of a chamber conditioned by a mixed air supply system that recirculates and conditions the room air. The chamber has inner dimensions of 2.5 × 2.75 × 2.8 m with two identical supply diffusers located at 2.0 m above floor level. The supply diffusers have a cross sectional area of 0.57 m (width) × 0.37 m (height). The exhaust diffuser is located at the adjacent wall at 0.53 m above floor level, it has a cross sectional area of 0.524 m (width) × 0.52 m (height).

In this chamber, the thermal manikin “Newton” manufactured by the Northwestern measured technology is used [28] (Fig. 5). This

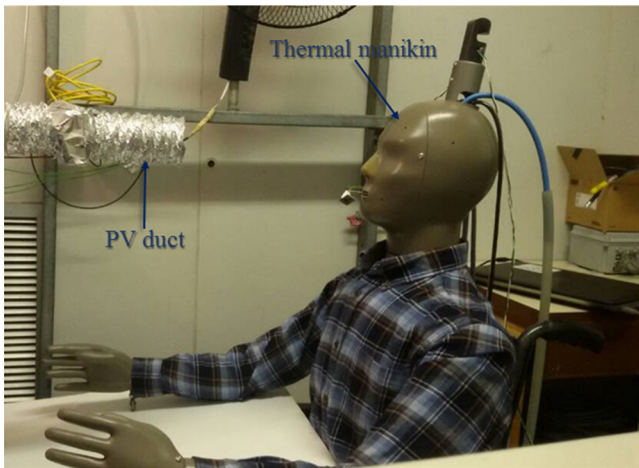


Fig. 5. Photo of thermal manikin and PV used in the experiment.

manikin is characterized by high performance of ± 0.1 °C temperature measurement and set-point control with a maximum power output range from 0 to 700 W/m². “Newton” is subdivided into twenty different control zones where each zone can report the segmental surface temperature based on assigned constant heat flux. “Newton” is controlled through “ThermDAC” control software that is user-friendly Windows-based application providing all possibilities of control. An internal load of 30 W/m² was generated in the room resulting in 135 W, and thermal manikin generating 100 W resulting in a total of 235 W. At a distance of 0.4 m from the manikin and at a 1.1 m height from the floor, a personalized venti-

lation nozzle of diameter 0.05 m is installed, the nozzle withdraws conditioned fresh air from a twin chamber and supplies it towards the occupant.

To study the ability of PV in delivering fresh air to the occupant, a constant source of CO₂ was placed at each wall to create uniform conditions inside the room. 4 sources of CO₂ deliver a constant flow rate of 2 L/min (each source delivering 0.5 L/min), the source of CO₂ represents passive contaminants generated in the room. CO₂ sensors were used to measure the concentration at different positions in the space. The sensors used were the FIGARO CDM7160 CO₂ sensor module having a detection range of 300–5000 ppm, and having an accuracy of ± 50 ppm. They were placed at the PV and mixing supplies and exhaust diffusers and in the breathing zone at 2.5 cm away from the manikin’s face. (See Fig. 6(a)) and connected to OMEGA DacPro data logger to store the data and check stabilized residuals.

2.3.1. Obtaining sinusoidal airflow

In order to create the sinusoidal airflow, a variable speed fan having dimensions of 80 mm (length) \times 80 mm (width) \times 25.4 mm (height) was placed inside the PV duct. The fan has a maximum DC voltage of 12 V and maximum power of 6.25 W.

The PV fan was controlled using LabVIEW software which takes the time and frequency as inputs and supplies the fan with a sinusoidal voltage. Accordingly, the fan can generate sinusoidal airflow with different fluctuation frequencies and different average flowrates. The two latter parameters are chosen according to typical values used in indoor spaces. The PV fan was placed in the duct away from the nozzle outlet. The fan flow circulated through the PV duct and measures were taken to straighten the flow before being supplied. To reduce swirling effect, flow turbulence intensity

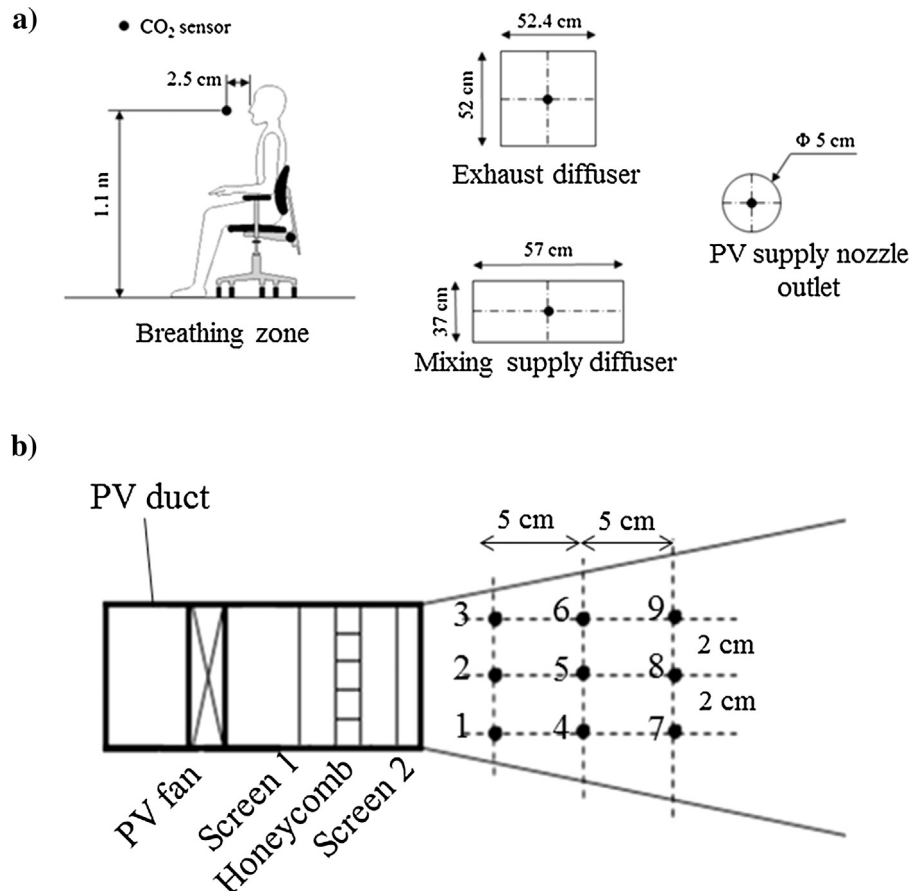


Fig. 6. a) Locations of CO₂ sensors: b) different velocity measurement positions of the PV jet decay.

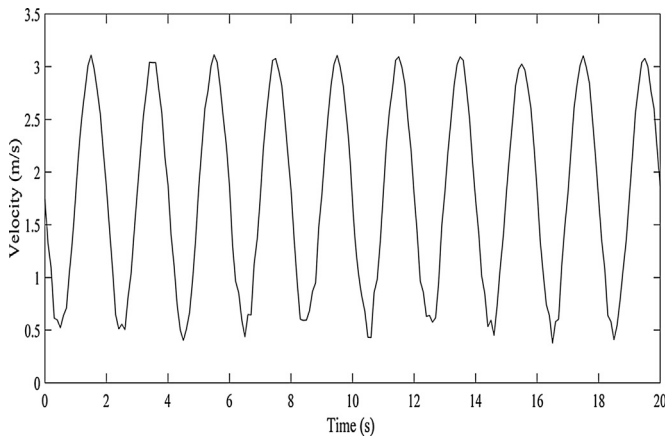


Fig. 7. Velocity profiles at a frequency 0.5 Hz and 3.5 L/s used in the CFD model.

and airflow mixing, a honeycomb flow straightener sandwiched between two screens was placed downstream inside the duct after the fan (see Fig. 1(b)). The honeycomb is 30 mm thick and has holes which diameter is equal to 4 mm such that the thickness over diameter ratio (t/D) is equal to 7.5 which gives optimal results [29]. A similar approach was adopted by Makhoul et al. [8]. In order to make sure that the swirl effect was minimized, velocity measurements along different distances from the PV outlet were taken as seen in Fig. 6(b) using an omnidirectional hot wire anemometer (OMEGA HHF2005HW model characterized by an accuracy of ± 0.5 °C for temperature and $\pm 10\%$ of full scale velocity measurement, ranging between 0.2 m/s and 20 m/s).

The velocity profiles and turbulence values obtained from measurements are then taken as input into the CFD model. The velocity profiles and turbulence values obtained from measurements are then taken as input into the CFD model. As an illustration, Fig. 7 shows the variation with time of the measured outlet PV jet velocity for a frequency of 0.5 Hz and an average flowrate of 3.5 L/s. Comparison will be made with CFD simulation results that assume an axial round PV jet exiting the nozzle to make sure that the swirl effect is negligible.

2.4. Experimental protocol

Initiating experiments begins by turning on the MV system and the lights in the chamber, and setting the manikin to a constant heat flux representing sedentary activity of 39 W/m². The flow rate and temperatures are set to 80 L/s and 28 °C respectively, then the CO₂ source is introduced into the room. Before turning on the personalized ventilation, the MV system, thermal manikin and CO₂ sources were operated for 3 h until reaching steady state conditions and the segmental skin temperatures of the manikin reached stable values.

After reaching steady state with the standalone mixing system, the PV system was turned on and it supplied cool fresh air at 24 °C under a sinusoidal pattern horizontally towards the thermal manikin at an average flowrate of 3.5 L/s. The CO₂ concentrations in the supplied fresh air were equal to 449 ppm. The averaged skin temperatures and CO₂ concentrations were monitored until stabilization. The experiment was repeated several times for accuracy.

3. Results and discussion

3.1. CFD validation

The CFD validation was performed for the conditions of the experiment at a room temperature of 28 °C and a PV jet of 24 °C supplying an intermittent flowrate of average 3.5 L/s. Three fre-

Table 2

Measured and predicted values of PV jet velocities in m/s for different positions shown in Fig. 6(b) along the PV jet.

Position	Experimentally measured velocity \pm Standard Deviation (m/s)	Predicted CFD velocity (m/s)
1	2.6 \pm 0.21	2.38
2	3.3 \pm 0.22	3
3	2.6 \pm 0.21	2.38
4	2.3 \pm 0.22	2.11
5	2.8 \pm 0.23	2.72
6	2.3 \pm 0.21	2.12
7	1.4 \pm 0.22	1.51
8	2.3 \pm 0.23	2.44
9	1.3 \pm 0.24	1.53

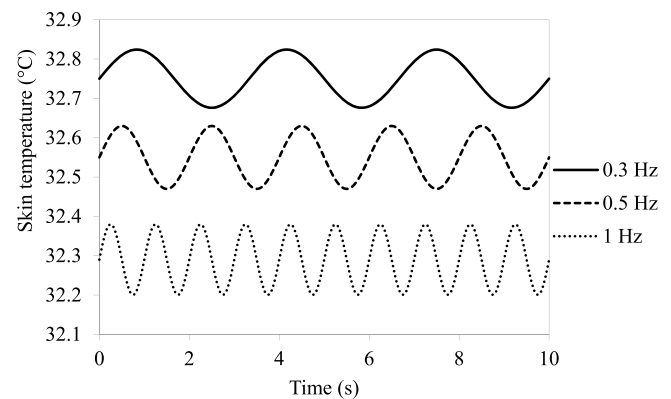


Fig. 8. Variation of head temperature for an average flowrate of 3.5 L/s and with frequencies of 0.3 Hz, 0.5 Hz and 1 Hz.

quencies were tested experimentally: 0.3 Hz, 0.5 Hz and 1 Hz. The CFD validation is done based on comparison between predicted and measured values of PV jet velocities at different positions, segmental skin temperatures and ventilation efficiency ϵ_v . The predicted and measured values of PV jet velocities for different positions can be seen in Table 2. There was agreement between measured and predicted values with a maximum relative error of 8.46% at position 3 indicating that the flow can be considered as a round axial flow with reduced turbulence and swirl.

The bio-heat and CFD models predict instantaneous values of segmental skin temperatures (see Fig. 8) and the CO₂ concentrations. However, the thermal manikin and CO₂ sensors cannot capture the instantaneous response at high frequencies due to the limitations of their response times. In fact, the CO₂ sensors have a long response time of 2 min whereas to capture a transient response from the thermal manikin, the operating period was lowered to 19 s corresponding to a frequency of 0.056 Hz. This frequency is outside the range of indoor frequencies which is why it wasn't included in the validation. Therefore, the validation was based on the predicted and measured values of the average segmental skin temperatures and average ventilation efficiencies.

The average segmental skin temperatures for the considered experimental conditions are presented in Fig. 9. When the PV fan was turned on supplying an intermittent jet flow, it was able to reduce the average skin temperature of the face from 34.5 °C to averages of 32.7 °C, 32.5 °C and 32.1 °C for 0.3 Hz, 0.5 Hz and 1 Hz respectively (Fig. 8) [28]. This is due to the increase of the convective currents at the head level and therefore heat loss from that segment. The results showed good agreement between predicted and measured segmental surface temperatures with relative errors ranging between 1.84% and 3.34% as can be seen in Fig. 9.

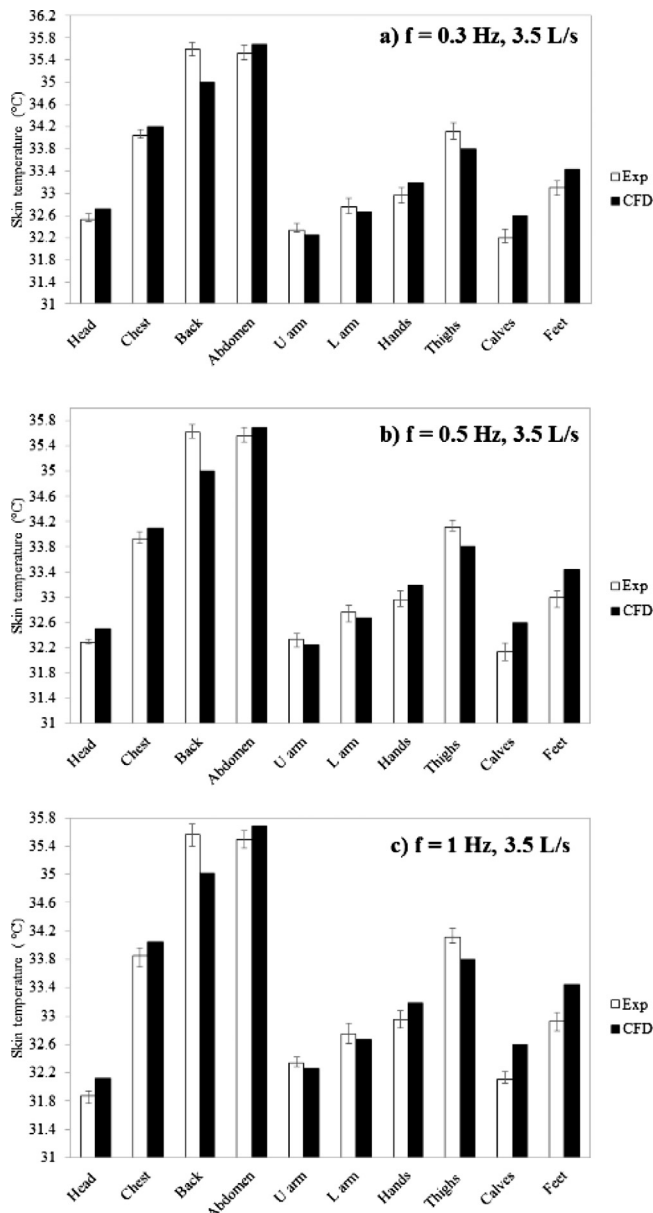


Fig. 9. Segmental surface temperature validation for an average flowrate of 3.5 L/s and 3 different frequencies.

The air quality is assessed using the ventilation efficiency (ε_v) parameter. The results are shown in Fig. 10 for 0.3 Hz, 0.5 Hz and 1 Hz. When increasing the frequency, there are two competing effects, the enhanced turbulence and the faster supply of fresh air to the BZ. For instance, with an increase in frequency from 0.3 Hz to 0.5 Hz, ventilation efficiency improved from 66.7% to 75.71%. However, when frequency further increased to 1 Hz, the efficiency degraded from 75.51% to 70.12% due to increased turbulence intensity at higher frequency which overcame the faster supply of fresh air. As a matter of fact, turbulence increased in the BZ by 13.71% and 26.25% when increasing the frequency from 0.3 Hz to 0.5 Hz and from 0.5 Hz to 1 Hz respectively. Results showed good agreement between experimental and predicted values with relative errors ranging between 1.94% and 5.7% with the standard deviation bars representing the experimental variations obtained from repeating each experiment several times (Fig. 10).

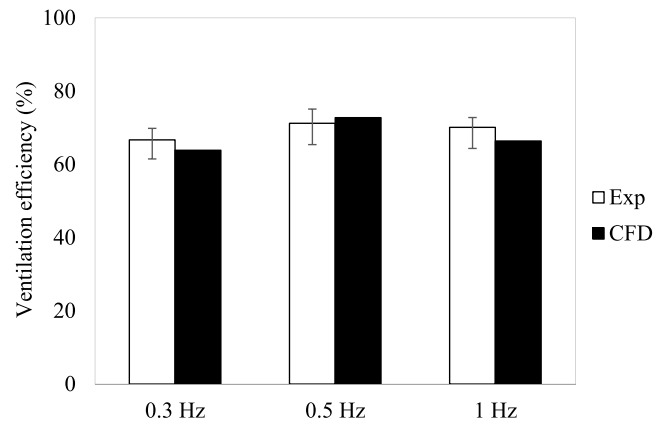


Fig. 10. Ventilation efficiency ε_v validation for an average flowrate of 3.5 L/s at frequencies of a) 0.3 Hz b) 0.5 Hz c) 1 Hz.

3.2. Parametric study

The main parameters affecting comfort and IAQ of the studied case are the PV average flowrate and fluctuation frequency. For this reason, a parametric study was conducted on a typical office space to study their effect on thermal comfort, air quality and energy savings.

A typical office space with inner dimensions of 3.4 m \times 3.4 m \times 2.8 m with supply and exhaust grills having a cross sectional area of 0.7 m (width) \times 0.3 m (length) and 0.5 m (width) \times 0.2 m (length) respectively was considered as was shown in Fig. 2. The PV outlet has a diameter of 0.05 m [7] and is fixed at a distance of 0.4 m from the manikin which is a typical separation distance between a PV device and an occupant in an office space [16]. A load of 40 W/m² distributed between lighting, walls, and occupancy, is set in the room. The MV system supplies 63 L/s of air at 20 °C assuring a set point temperature of 26 °C inside the space. The temperature of the dynamic airflow exiting the PV is set 22 °C [24]. Four CO₂ sources are introduced into the room, each supplying 0.5 L/min through a tube to ensure a uniform distribution of passive contaminants within the room.

In order to optimize the frequency and the average flowrate of the PV jet, 3 sets of simulations were conducted. The PV fan was operated at three different frequencies (0.3 Hz, 0.5 Hz and 1 Hz), and average flowrates (3.5 L/s, 5 L/s and 7.5 L/s). To determine PV minimum flowrate allowing the penetration of the thermal plumes, simulations were performed with Fluent. The minimal velocity obtained for a PV of diameter 0.05 m and situated at a distance of 0.4 m from the occupant was $V_1 = 0.5$ m/s. The contours of temperature for this case can be seen in Fig. 11, the PV jet was able to penetrate the thermal plume. It is important to note that the thermal plume penetration assessment depends on how precise the body shape is simulated. In this study, the manikin geometry used in the CFD model mimics the body profile of a typical average person having a total surface area of 1.8 m² close to the average human body area. Once the average and minimum velocities are determined, the maximum velocities at the PV nozzle exit are known and they are equal to 3.0 m/s, 4.5 m/s and 7.0 m/s for the three average flowrates respectively. It is noteworthy that the velocities near the face for the maximum PV flowrate were nearly 1 m/s, 1.2 m/s and 2 m/s respectively. Velocities were further reduced at close proximity to the eye due to the presence of the rising thermal plume. Nevertheless, the transient pattern tolerates for higher velocities to reach the face level with less risk of eye discomfort [30].

The combination of frequencies and average flowrates resulted in 9 test cases that were simulated as summarized in Table 3. For each case, the bio-heat model was simulated until quasi steady

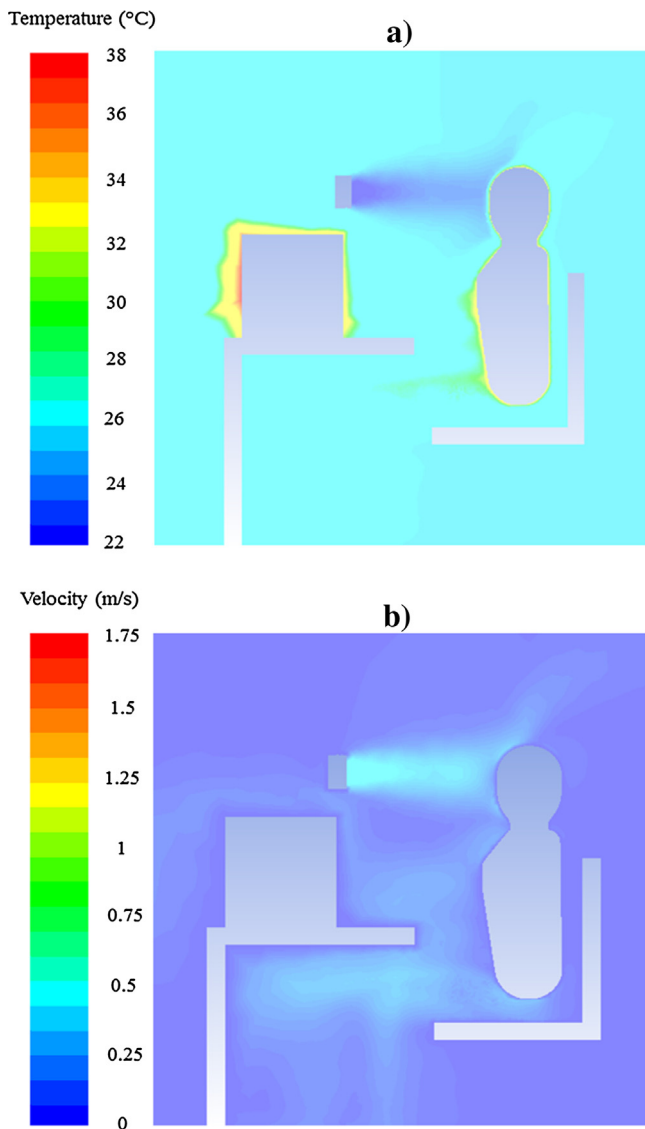


Fig. 11. Temperature field for a minimum flowrate of 1 L/s.

Table 3

Different simulation cases at a background temperature of 26 °C and PV jet temperature of 22 °C.

	Average flowrate (L/s)	Frequency (Hz)
Set 1	3.5 L/s	0.3 Hz
		0.5 Hz
		1 Hz
Set 2	5 L/s	0.3 Hz
		0.5 Hz
		1 Hz
Set 3	7.5 L/s	0.3 Hz
		0.5 Hz
		1 Hz

state conditions were reached to obtain the transient segmental skin temperatures, thermal sensation and thermal comfort.

3.2.1. Effect of fluctuation frequency and average flowrate

3.2.1.1. Thermal comfort. The effect of fluctuation frequency and average flowrate on thermal comfort was investigated. Tables 4 and 5 summarize the results for the overall thermal sensation (OTS) and overall thermal comfort (OTC) for different fluctuation frequencies and average flowrates. For a fixed average

Table 4

Overall thermal sensation at different wind frequencies and different average flowrates.

PV Flow Rate Frequency (Hz)	Ta = 26 °C, PV jet temperature = 22 °C, RH = 50%		
	3.5 L/s	5 L/s	7.5 L/s
0.3 Hz	0.366	0.334	0.272
0.5 Hz	0.262	0.12	-0.226
1 Hz	0.163	0.1	-0.32

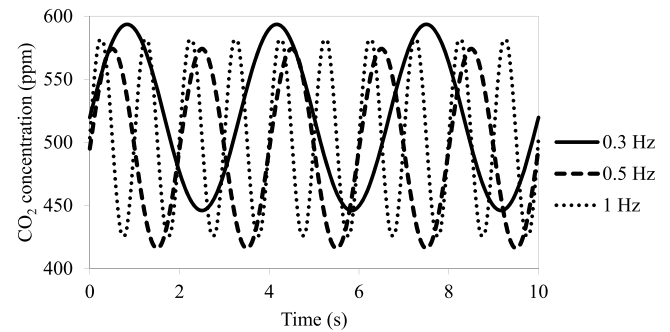


Fig. 12. Variation of head temperature for an average flowrate of 3.5 L/s and with frequencies of 0.3 Hz, 0.5 Hz and 1 Hz.

flowrate, when increasing frequency, the OTS decreases and OTC improves. This trend is observed for all flowrates. The decrease in OTS and improvement in OTC with higher frequencies is due to an increase in the convective currents near the head leading to lower head temperatures and higher rates of change. For instance, at an average flowrate of 3.5 L/s, the OTS decreases from 0.366 to 0.163 and the OTC increases from 0.325 (just comfortable) to 0.704 (comfortable) [21–23] when the frequency increases from 0.3 Hz to 1 Hz. For this case, the average face skin temperature decreased from 34.28 °C to 33.82 °C and the average rate of change increased from 0.089 °C/s to 0.296 °C/s when the frequency increased from 0.3 Hz to 1 Hz.

In addition, when increasing the average flowrate, the OTS decreased for all frequencies. However, the OTC increased with flowrate just for the first two frequencies (0.3 Hz and 0.5 Hz). On the other hand, at a frequency of 1 Hz, the highest recorded OTC was obtained at 5 L/s. In fact, at a flowrate of 7.5 L/s, the increased convective air currents due to the combination of high frequency and flowrate led to overcooling of the head resulting in thermal draft (Tables 4–5).

3.2.1.2. Indoor air quality. It was shown that localized dynamic air-flow gave good values of comfort. However, a transient PV fresh air profile might be challenging in providing good IAQ. In fact, transient flows create more turbulence than steady flows resulting in higher mixing between the PV jet and the surrounding air. In addition, when the flowrate reaches a minimum, not enough fresh air is diluting the contaminants in the BZ of the occupant.

Due to intermittent PV jet, the CO₂ concentration is transient in the BZ and fluctuates between a minimum and a maximum as can be seen in Fig. 12. The CO₂ concentration profile is maximal when the minimum flowrate is supplied and is minimal when the maximal flowrate is delivered.

When increasing the frequency of an intermittent flow, the air is supplied at a faster rate and at the same time turbulence is enhanced due to faster fluctuations. Therefore, there are two competing effects that affect air quality: turbulence and rate of supply. Results show that when increasing frequency from 0.3 Hz to 0.5 Hz at a fixed average flowrate, the general CO₂ concentrations profile

Table 5
Overall thermal comfort at different wind frequencies and different average flowrates.

PV Flow Rate Frequency (Hz)	Ta = 26 °C, PV jet temperature = 22 °C, RH = 50%		
	3.5 L/s	5 L/s	7.5 L/s
0.3 Hz	0.325	0.334	0.341
0.5 Hz	0.418	0.4812	0.4966
1 Hz	0.704	1.2843	1.015

Table 6
Minimum and maximum ventilation efficiencies ε_v (%) at 3 frequencies and 3 average flowrates at background temperature of 26 °C and a PV jet temperature of 22 °C.

	[Minimum, Maximum] ε_v (%)		
	3.5 L/s	5 L/s	7.5 L/s
0.3 Hz	[20.62, 76.84]	[22.6, 81.62]	[55.94, 85.43]
0.5 Hz	[21, 92.6]	[30.33, 93.63]	[59.23, 96.23]
1 Hz	[19.36, 84.1]	[26.45, 90.63]	[58.84, 94.89]

decreases leading to increase of minimum and maximum ventilation efficiencies (Table 5). Therefore, increasing the frequency of fresh air supply from 0.3 Hz to 0.5 Hz for all average flowrates was able to overcome the increasing turbulence effect in the occupant BZ which according to the simulations increased by a value of 13.53% for an average flowrate of 3.5 L/s. On the other hand, when further increasing frequency to 1 Hz, the general CO₂ concentrations profile increased and minimum and maximum ventilation efficiencies ε_v decreased (see Table 6). In this case, the turbulence effect overcame the positive impact of larger supply of fresh air. As a matter of fact, the turbulence intensity in the BZ increased by 25.93% when increasing the frequency from 0.5 Hz to 1 Hz at 3.5 L/s. This behavior was observed for all average flowrates (see Table 6 and Fig. 12).

When increasing the average flowrate at a fixed frequency, the [minimum and maximum] CO₂ concentrations decreased leading to higher ventilation efficiencies ε_v (Table 6). This is due to the increase quantity of fresh air reaching the BZ. This trend is observed for all frequencies. For instance, at 0.5 Hz, when increasing the average flowrate from 3.5 L/s to 7.5 L/s, the CO₂ concentrations decreased from [418.5, 597.5] ppm to [409.43, 501.93] ppm (see Fig. 12) and ventilation efficiencies ε_v increased from [21, 92.6] % to [59.23, 96.23] % (see Table 6).

3.2.1.3. Frequency optimization. It was shown previously that the different combinations of fluctuation frequency and average flowrate supplied by the PV affect thermal comfort and air quality. Increasing frequency increased thermal comfort for all average flowrates, however for a frequency larger than 0.5 Hz, the air quality was compromised.

Therefore, it is of interest to find an optimal operating frequency that could provide the best combination of OTC and ventilation efficiency ε_v . Accordingly and after several simulations at different frequencies, these two indices (average OTC and average ε_v) were plotted as function of frequency at the three different average flowrates 3.5 L/s, 5 L/s and 7.5 L/s as shown in Fig. 13(a)–(c) respectively. The optimal frequency is selected based on the intersection between these two indices. It can be deduced from Fig. 13 that the optimal operating frequency would be 0.76 Hz, 0.86 Hz, and 0.94 Hz for 3.5 L/s, 5 L/s and 7.5 L/s, respectively. The optimal frequency range is between 0.5–1 Hz which is consistent with the range found by Huang et al. [27] and it increased with the increase in PV jet average flowrate. In addition, the ventilation effectiveness decreased when the frequency increased from 0.5 Hz to 1 Hz for all average flowrates. According to Fig. 13, this decrease is less

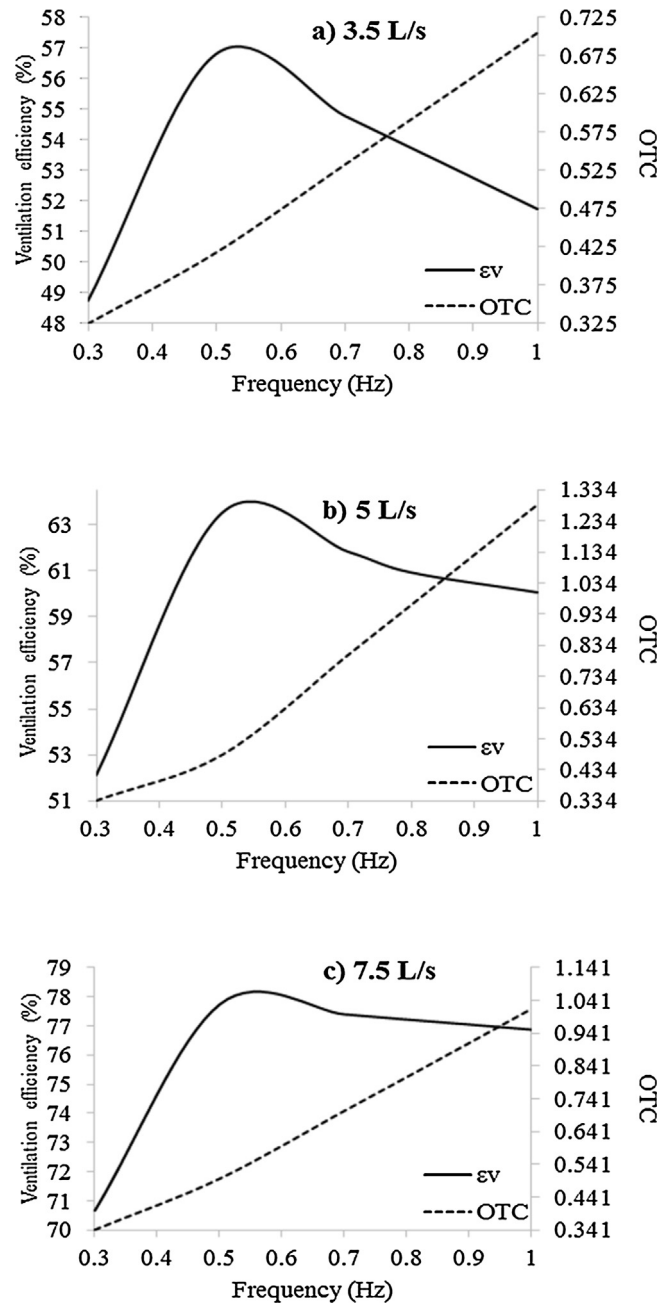


Fig. 13. Fluctuation of CO₂ concentrations in the occupant BZ for 0.3 Hz, 0.5 Hz and 1 Hz for a fixed flowrate of 5 L/s.

significant when operating with higher average flowrates. Due to the smaller decrease in effectiveness with the increase of average flowrate, the point of intersection between the curve of OTC and effectiveness shifted towards higher frequencies. Therefore the optimal frequencies increased with higher flowrates. An optimal operating case between the three average flowrates would be to use an average of 7.5 L/s, with an operating frequency of 0.94 Hz, since it provided the best ventilation efficiency (77%) and a good level of comfort (0.95) (comfortable) [21–23]. An additional advantage of the sinusoidal flow profile is the oscillatory effect which according to Melikov et al. [31] leads to less eye discomfort than a constant blowing fan flow and could offset the increase in velocity at the face.

3.2.2. Energy savings

It has previously been shown that a PV system operating with an intermittent flow at a frequency of 0.94 Hz and an average flowrate of 7.5 L/s provided both comfortable conditions (0.9) [21–23] and acceptable air quality ($\varepsilon_v = 77\%$). It is expected that the same PV system operating with a constant flowrate would assure same comfort but at higher energy cost. Therefore it is of importance to check the energy savings provided by an intermittent flow PV system.

To evaluate energy savings, the optimal case was compared to constant PV airflow. A constant flow PV system cannot simultaneously satisfy the same comfort and air quality provided by the intermittent flow. Consequently, 2 sets of steady state simulations were performed to find

- (i) the constant flowrate that assured same OTC of 0.95 (comfortable) and
- (ii) the constant flowrate that provided the same average ventilation efficiency as the optimal intermittent flow.

For case (i), it was found that constant PV flowrate 9 L/s was able to provide the same OTC value of 0.95 (comfortable) as that of the intermittent PV at average flow rate of 7.5 L/s. Therefore, a higher constant PV flowrate was needed to provide the same level of comfort as the intermittent PV. In addition, it is expected that a flowrate of 9 L/s will be able to provide higher air quality than the intermittent PV. As a matter of fact, the ventilation efficiency recorded a value of 95.48% which is much higher than the IAQ requirements and according to Melikov et al. [24], high values of ventilation efficiency (almost 100%) were obtained when operating with a constant PV flowrate of 10 L/s. However, satisfactory levels ($\varepsilon_v = 77\%$) were also achieved with an intermittent flow with the advantage of less energy cost. The optimized intermittent PV flow allowed reaching a compromise between thermal comfort, IAQ and energy cost.

For case (ii), it was found that a constant flowrate of 5.6 L/s was able to provide the same level of air quality ($\varepsilon_v = 77\%$) as the intermittent flow. The obtained flowrate is smaller than the average flowrate of the intermittent flow (7.5 L/s). This is expected since a constant flowrate delivers fresh air continuously in the BZ with minimal turbulence in the BZ and hence not the same amount of fresh air is needed to achieve acceptable levels of air quality. However, this constant flowrate was not able to provide the same level of comfort (OTC=0.4, just comfortable) as that of the intermittent flow, since the PV jet cannot penetrate the human thermal plume and cool the head as effectively as the higher jet velocities.

Thus, the intermittent PV flow (0.94 Hz, 7.5 L/s) was able to provide good comfort and good ventilation efficiency compared to a constant PV flow (9 L/s). In both cases, the fresh air is cooled by using the same chiller. To calculate the energy savings, the cooling capacity of each system as well as the fan power consumption for steady and transient operation were computed.

The PV fan operating at steady state conditions with a constant flowrate of 9 L/s is considered as the reference case with a nominal power of 1.62 W. To calculate the PV fan power consumptions in the case of transient operation at the optimal frequency of 0.94 Hz. The correlation of Keblawi et al. [32] was used:

$$P_{fan} = P_{reference} \left(\frac{\dot{m}_a}{\dot{m}_{a,reference}} \right)^3 \quad (3)$$

Where P_{fan} is the fan power consumption and \dot{m}_a is the mass flow rate of the fan, $P_{reference}$ and $\dot{m}_{a,reference}$ are the nominal power consumption and mass flowrate respectively considered for the steady

state PV operation. For transient operation, the fan power was computed over a period according to the following equation:

$$P_{fan} = \frac{1}{T} \int_0^T P_{reference} \left(\frac{\dot{m}_a}{\dot{m}_{a,reference}} \right)^3 dt$$

Where T is one period of oscillation. The obtained fan power consumption for transient operation at the optimal frequency might be slightly larger than the consumption for steady state operation.

The fan power consumption was calculated for transient operation for the optimal frequency of 0.94 Hz and results showed that it is higher than the nominal fan power for steady state by 18.69%. As for the cooling capacity, results showed that the cooling capacity for transient condition decreased by 16.67% compared to steady state conditions. However, for a small nominal power of the fan of 1.62 W, the transient fan power consumption was 2 W with a small different of nearly 0.4 W. As for the cooling capacity, for a difference between outside temperature and supply temperature of 10 °C at a relative humidity of 50%, the transient PV operation spent 92 W while the steady state operation spent nearly 111 W. Therefore the decrease in cooling capacity was more significant than the increase in fan power consumption between transient and steady state PV operation. Therefore a transient PV system operating at an average flowrate of 7.5 L/s and a frequency of 0.94 Hz resulted in energy savings of 16.1%.

4. Conclusion

A validated transient 3D CFD model is integrated with a transient bio-heat model to select the optimal fluctuation frequency of a PV oscillating flow that can provide acceptable thermal comfort and good IAQ with the least energy consumption. This was done through variation of fluctuation frequency based on values used in indoor spaces, and through variation of the PV fan average flow rate. The interrelation between these parameters and their effect on thermal comfort and IAQ led to an optimal frequency of 0.94 Hz and an average flowrate of 7.5 L/s. In addition, energy analysis revealed that for these operating conditions of the intermittent PV system, energy savings of 21.34% were recorded compared to constant flow PV system providing same levels of comfort.

Acknowledgement

The financial of the University Research Board at the American University of Beirut through grant Award No. 103371/23303 is greatly acknowledged.

References

- [1] B. Tashtoush, M. Molhim, M. Al-Rousan, Dynamic model of an HVAC system for control analysis, *Energy* 30 (2005) 1729–1745, <http://dx.doi.org/10.1016/j.energy.2004.10.004>.
- [2] B. Yu, Z. Hu, M. Liu, H. Yang, Q. Kong, Y. Liu, Review of research on air-conditioning systems and indoor air quality control for human health, *Int. J. Refrig.* 32 (2009) 3–20, <http://dx.doi.org/10.1016/j.ijrefrig.2008.05.004>.
- [3] B. Halvoňová, A.K. Melikov, Performance of ductless personalized ventilation in conjunction with displacement ventilation: impact of intake height, *Build. Environ.* 45 (2010) 996–1005, <http://dx.doi.org/10.1016/j.buildenv.2009.10.007>.
- [4] R. Li, S. Sekhar, A. Melikov, Thermal comfort and IAQ assessment of under-floor air distribution system integrated with personalized ventilation in hot and humid climate, *Build. Environ.* 45 (2010) 1906–1913, <http://dx.doi.org/10.1016/j.buildenv.2010.03.003>.
- [5] S.C. Sekhar, N. Gong, K.W. Tham, K.W. Cheong, A.K. Melikov, D.P. Wyon, et al., Findings of personalized ventilation studies in a hot and humid climate, *HVAC&R Res.* 11 (2005) 603–620, <http://dx.doi.org/10.1080/10789669.2005.10391157>.
- [6] B. Yang, C. Sekhar, A.K. Melikov, Ceiling mounted personalized ventilation system in hot and humid climate—An energy analysis, *Energy Build.* 42 (2010) 2304–2308, <http://dx.doi.org/10.1016/j.enbuild.2010.07.022>.

- [7] A. Makhoul, K. Ghali, N. Ghaddar, Low-mixing coaxial nozzle for effective personalized ventilation, *Indoor Built Environ.* 24 (2015) 225–243, <http://dx.doi.org/10.1177/1420326x13508967>.
- [8] A. Makhoul, K. Ghali, N. Ghaddar, Desk fans for the control of the convection flow around occupants using ceiling mounted personalized ventilation, *Build. Environ.* 59 (2013) 336–348, <http://dx.doi.org/10.1016/j.buildenv.2012.08.031>.
- [9] S. Schiavon, A.K. Melikov, C. Sekhar, Energy analysis of the personalized ventilation system in hot and humid climates, *Energy Build.* 42 (2010) 699–707, <http://dx.doi.org/10.1016/j.enbuild.2009.11.009>.
- [10] K. Ghali, N. Ghaddar, M. Bizri, The influence of wind on outdoor thermal comfort in the city of Beirut: a theoretical and field study, *HVAC&R Res.* (2011) 813–828, <http://dx.doi.org/10.1080/10789669.2011.607746>.
- [11] A. Kabanshi, H. Wigö, M. Sandberg, Experimental evaluation of an intermittent air supply system –Part 1: Thermal comfort and ventilation efficiency measurements, *Build. Environ.* 95 (2016) 240–250, <http://dx.doi.org/10.1016/j.buildenv.2015.09.025>.
- [12] A. Ugursal, C.H. Culp, The effect of temperature, metabolic rate and dynamic localized airflow on thermal comfort, *Appl. Energy* 111 (2013) 64–73, <http://dx.doi.org/10.1016/j.apenergy.2013.04.014>.
- [13] S. Tanabe, K. Kimura, Effects of air temperature, humidity, and air movement on thermal comfort under hot and humid conditions, in: No. CONF-9406105, *American Society of Heating, Refrigerating and Air-Conditioning Engineers, Inc.*, Atlanta, 2017.
- [14] G. Zhou, A. Melikov, P.O. Fanger, Impact of equivalent frequency on the sensation of draught, in: *Proceedings of Roomvent, September, Copenhagen, Denmark, 2002*, pp. 297–300.
- [15] J. Kaczmarczyk, A. Melikov, D. Sliva, Effect of warm air supplied facially on occupants' comfort, *Build. Environ.* 45 (2010) 848–855, <http://dx.doi.org/10.1016/j.buildenv.2009.09.005>.
- [16] M. Kanaan, N. Ghaddar, K. Ghali, Simplified model of contaminant dispersion in rooms conditioned by chilled-Ceiling displacement ventilation system, *HVAC&R Res.* 16 (2010) 765–783, <http://dx.doi.org/10.1080/10789669.2010.10390933>.
- [17] A. Melikov, J. Kaczmarczyk, Measurement and prediction of indoor air quality using a breathing thermal manikin, *Indoor Air* 17 (2007) 50–59, <http://dx.doi.org/10.1111/j.1600-0668.2006.00451.x>.
- [18] ANSYS Fluent User's Guide, ANSYS Inc. Southpointe, Canonsburg, PA, USA, 2017.
- [19] W.A. Hweij, N. Ghaddar, K. Ghali, C. Habchi, Optimized performance of displacement ventilation aided with chair fans for comfort and indoor air quality, *Energy Build.* 127 (2016) 907–919, <http://dx.doi.org/10.1016/j.enbuild.2016.06.052>.
- [20] M. Al-Othmani, N. Ghaddar, K. Ghali, A multi-segmented human bioheat model for transient and asymmetric radiative environments, *Int. J. Heat Mass Transfer* 51 (2008) 5522–5533, <http://dx.doi.org/10.1016/j.ijheatmasstransfer.2008.04.017>.
- [21] H. Zhang, E. Arens, C. Huizenga, T. Han, Thermal sensation and comfort models for non-uniform and transient environments: part I: Local sensation of individual body parts, *Build. Environ.* 45 (2010) 380–388, <http://dx.doi.org/10.1016/j.buildenv.2009.06.018>.
- [22] H. Zhang, E. Arens, C. Huizenga, T. Han, Thermal sensation and comfort models for non-uniform and transient environments, part II: Local comfort of individual body parts, *Build. Environ.* 45 (2010) 389–398, <http://dx.doi.org/10.1016/j.buildenv.2009.06.015>.
- [23] H. Zhang, E. Arens, C. Huizenga, T. Han, Thermal sensation and comfort models for non-uniform and transient environments, part III: Whole-body sensation and comfort, *Build. Environ.* 45 (2010) 399–410, <http://dx.doi.org/10.1016/j.buildenv.2009.06.020>.
- [24] A.K. Melikov, R. Cermak, M. Majer, Personalized ventilation: evaluation of different air terminal devices, *Energy Build.* 34 (2002) 829–836, [http://dx.doi.org/10.1016/s0378-7788\(02\)00102-0](http://dx.doi.org/10.1016/s0378-7788(02)00102-0).
- [25] Y. Zhu, Q. Ouyang, B. Cao, X. Zhou, J. Yu, Dynamic thermal environment and thermal comfort, *Indoor Air* 26 (2015) 125–137, <http://dx.doi.org/10.1111/ina.12233>.
- [26] P.O. Fanger, C.J.K. Pederson, Discomfort due to air velocities in spaces, *Proceedings of the Meeting of Commission B. B1, B2, E1 of the International Institute of Refrigeration 4 (1977)* 289–296.
- [27] L. Huang, Q. Ouyang, Y. Zhu, Perceptible airflow fluctuation frequency and human thermal response, *Build. Environ.* 54 (2012) 14–19, <http://dx.doi.org/10.1016/j.buildenv.2012.02.004>.
- [28] Instruments for Textile & Biophysical Testing Brochure: Newton Thermal Manikin System. Thermetrics Inc. Advanced Thermal Measurement Technologies, Seattle, WA, USA, 2015.
- [29] V. Kulkarni, N. Sahoo, S.D. Chavan, Simulation of honeycomb-screen combinations for turbulence management in a subsonic wind tunnel, *J. Wind Eng. Ind. Aerodyn.* 99 (2011) 37–45, <http://dx.doi.org/10.1016/j.jweia.2010.10.006>.
- [30] P. Wolkoff, Eye complaints in the office environment: precorneal tear film integrity influenced by eye blinking efficiency, *Occup. Environ. Med.* 62 (2005) 4–12, <http://dx.doi.org/10.1136/oem.2004.016030>.
- [31] A.K. Melikov, T. Sakoi, S. Kolencíková, N. Tominaga, Impact of air movement on eye symptoms, in: *Proceedings of 11th REHVA World Congress and the 8th International Conference on Indoor Air Quality, Ventilation and Energy Conservation in Buildings [959]*, Prague, Czech Republic, on June 16–19, 2013, 2013.
- [32] A. Keblawi, N. Ghaddar, K. Ghali, Model-based optimal supervisory control of chilled ceiling displacement ventilation system, *Energy Build.* 43 (2011) 1359–1370, <http://dx.doi.org/10.1016/j.enbuild.2011.01.021>.